Title

Structure and Reactivity of a High-Spin, Nonheme Iron(III)- Superoxo Complex Supported by Phosphinimide Ligands

Journal

Journal of the American Chemical Society, 143(34)

ISSN

0002-7863

Authors

Winslow, Charles
Lee, Heui Beom
Field, Mackenzie J
et al.

Publication Date

2021-09-01

DOI

10.1021/jacs.1c05276

Peer reviewed

Structure and Reactivity of a High-Spin, Non-Heme Iron(III)- Superoxo Complex Supported by Phosphinimide Ligands

Charles Winslow[†], Heui Beom Lee[†], Mackenzie J. Field[‡], Simon J. Teat[§], and Jonathan Rittle[†,*]

† College of Chemistry, University of California Berkeley, Berkeley, California 94720, United States

‡ Department of Chemistry, University of California Irvine, Irvine, California 92697, United States

§ Advanced Light Source, Lawrence Berkeley National Laboratory, Berkeley, California 94720, United States

ABSTRACT: Non-heme iron oxygenases utilize dioxygen to accomplish challenging chemical oxidations. Further understanding of the Fe-O_2 intermediates implicated in these processes is challenged by their highly transient nature. To that end, we have developed a ligand platform featuring phosphinimide donors intended to stabilize oxidized, high-spin iron complexes. O_2 exposure of single crystals of a three-coordinate Fe(II) complex of this framework allowed for *in crystallo* trapping of a terminally-bound Fe-O_2 complex suitable for XRD characterization. Spectroscopic and computational studies of this species support a high-spin Fe(III) center antiferromagnetically coupled to a superoxide ligand, similar to that proposed for numerous non-heme iron oxygenases. In addition to the stability of this synthetic Fe-O_2 complex, its ability to engage in a range of stoichiometric and catalytic oxidation processes demonstrates that this iron-phosphinimide system is primed for development in modelling oxidizing bioinorganic intermediates and green oxidation chemistry.

Introduction

Dioxygen is the ideal chemical oxidant.[1] Enzymatic systems that effectively harness O_2, such as the large class of mononuclear non-heme iron oxygenases, are essential to myriad biological processes.[2] This particular class of enzymes catalyze an enormous range of O_2-dependent substrate oxidations that are increasingly recognized to proceed via pronounced mechanistic diversity.[3] Perhaps the only chemical events central to all of these enzymes is the coordination and activation of O_2 by the iron cofactor. Yet, discrete Fe-O_2 intermediates have proven to be highly transient or unobservable in most enzymes.[4–6] Moreover, synthetic examples of well-characterized, non-heme Fe-O_2 complexes remain scarce owing to their reactive nature.[7–9]

These enzymes have inspired numerous breakthroughs in the creation of synthetic catalysts for sustainable oxidation processes.[10–12] Molecular catalysts for selective C-H bond functionalization, alcohol oxidation and alkene epoxidation have been developed that possess structural and/or mechanistic features congruent with those of non-heme iron enzymes.[10] However, unlike the natural systems, most of these synthetic catalysts do not utilize O_2 directly and instead rely upon alternative oxidants - such as peroxides - which provide access to viable catalytic intermediates at the expense of increased cost or undesirable side reactivity.[13] Understanding and developing molecular systems that directly harness O_2 as a reagent could enable transformative advances in chemical oxidation catalysis.

We have initiated a research program that aims to develop new molecular catalysts for sustainable oxidative processes. Along these lines we have developed an electron-donating and oxidatively-resilient ligand platform featuring anionic phosphinimide donors intended to expand the reaction chemistry of Earth-abundant, first-row transition metals.[14] Herein, we show that this ligand enables the synthesis and characterization – including the XRD analysis – of a non-heme iron complex that binds O_2 in a terminal fashion. The available structural, spectroscopic, and computational data on this species corroborates a high-spin iron(III)-superoxide formulation which, in turn, is active in a diverse array of oxidation reactions, including catalytic O_2-mediated aldehyde deformylation.

Results and Discussion

Terminally-bound phosphinimides are weak-field, π-basic ligands isolobal to alkoxides.[15] They have most commonly been used to stabilize electron-deficient lanthanides and early transition metals.[16,17] In contrast, the coordination chemistry of these ligands with transition metals harboring substantial *d*-electron counts has not been intensively studied, owing in part to the propensity of phosphinimides to instead act as bridging ligands with electron-rich metal centers.[18,19] The ligand platform employed here features a rigid, sterically encumbering framework designed to preclude oligomerization and direct these ligands to a single metal ion. Scheme 1 details an abbreviated synthesis of our featured tris(phosphinimine) pro-ligand (**$L^{Ad}H_3$**) decorated with bulky 1-adamantyl substituents.

The **$L^{Ad}H_3$** pro-ligand supports an electron-rich mononuclear Fe(II) species. The combination of $Fe(HMDS)_2$ with **$L^{Ad}H_3$** results in the protonolysis of two phosphinimines yielding neutral **$(L^{Ad}H)Fe$** (Scheme 1). The solid-state structure of **$(L^{Ad}H)Fe$** features a trigonal planar iron atom bound to two phosphinimides and one phosphinimine (Fig 1). Observed Fe-N bond distances coincide with the protonation state of each donor atom: the two Fe-N(phosphini*mide*) bond distances are 1.886(2) and 1.894(2) Å whereas the Fe-N(phosphini*mine*) bond distance is 2.074(2) Å. The short Fe-N(phosphinimide) bond distances can be understood by the two canonical resonance forms of phosphinimide ligands (Scheme 2). Considering resonance form (B), terminal phosphinimide coordination to Fe allows for Fe-N σ-bonding and multiplanar Fe-N π-bonding. Such π-donation is expected to considerably raise the energy of the *d*-orbital manifold and stabilize high-spin ground states.

Solution-phase magnetic measurements of this compound are consistent with an $S = 2$ spin state ($\mu_{eff} = 4.94\ \mu_B$), as is typical for three-coordinate Fe^{II} compounds.[20,21] Electrochemical experiments indicate that **(L^{Ad}H)Fe** exhibits a quasi-reversible oxidation event at -1.35 V vs Fc/Fc^+ in THF electrolyte (Fig S17), which is significantly more reducing than related trigonal, high-spin iron(II) complexes.[22,23] We hypothesize that the unusually low oxidation potential of **(L^{Ad}H)Fe** is a testament to the π-donation presented by the terminally-bound phosphinimide ligands.

The **(L^{Ad}H)Fe** compound reacts with O_2 *in crystallo* to form a terminal Fe-O_2 complex, **(L^{Ad}H)FeO$_2$**. Yellow monoclinic crystals of **(L^{Ad}H)Fe** visibly darken to a red color upon exposure to dry O_2 at ambient temperature and retain strong diffraction intensity to ~0.8 Å. Subsequent XRD studies on one of these crystals at 100K using synchrotron radiation indicate that a single O_2 molecule has coordinated to the Fe center (Fig 1) which adopts a squashed-tetrahedral geometry ($THC_{DA} = 0.55$)[24] in **(L^{Ad}H)FeO$_2$**.[25] Despite the low coordination geometry at Fe, the O_2 ligand is bound in an ordered, terminal fashion with average measured Fe-O and O-O bond distances of 1.981(3) and 1.321(5) Å, respectively, and an Fe-O-O angle of 114.8(3)°. The observed O-O distance implies an activated superoxide (O_2^-) formulation (Supporting Information). Marginally shorter average Fe-N(phosphinimide) distances (1.87(2) Å) in **(L^{Ad}H)FeO$_2$** as compared to its precursor are also consistent with a more oxidized Fe center. To the best of our knowledge, this is the first crystallographically characterized, mononuclear non-heme iron-dioxygen complex obtained via addition of O_2 to a synthetic Fe(II) compound.[7,8] The terminal manner of O_2 coordination and the experimentally determined structural metrics are comparable to those computationally predicted for the Fe-O_2 adducts in isopenicillin N-synthase,[5] homoprotocatechuate dioxgenase,[4] and other non-heme iron oxygenases.[26–28]

Infrared spectra were collected on KBr pellets of isolated **(L^{Ad}H)FeO$_2$** to assess the vibrational characteristics of the O_2-derived ligand. According to a Badger's Rule analysis (Supporting Information), the lengthened O-O distance present in **(L^{Ad}H)FeO$_2$** should correlate with a ν(O-O) vibration of ~1030 cm^{-1}. A comparison of the FTIR spectra of **(L^{Ad}H)FeO$_2$** generated with ^{16}O- or ^{18}O-labelled O_2 reveal subtle differences in the range of 1050-1250 cm^{-1} (Fig S13). In contrast, the spectral features nearly overlay in the range commonly ascribed to metal-peroxo (O_2^{2-}) species (700-900 cm^{-1}).[29] The absence of a unique, isotopically-sensitive feature in **(L^{Ad}H)FeO$_2$** can be explained by coupling of the ν(O-O) vibration with the ν(P=N) vibrations from the adjacent phosphinimides. High-spin iron-phosphinimide complexes commonly display intense ν(P=N) modes in the range of 1050-1250 cm^{-1}.[30,31] After appropriate scaling,[32] our DFT results (*vide infra)* on **(L^{tBu}H)FeO$_2$** identify multiple vibrational modes with variable ν(O-O) and ν(P=N) character that span this spectral range. Upon ^{18}O-O_2 labelling, these studies predict an increase in spectral intensity at ~1240 and 1120 cm^{-1} with a concomitant decrease of intensity at ~1190 cm^{-1}, in modest agreement with the experimental data. Owing to the inherent complexity of this system, however, we cannot confidently assign a unique ν(O-O) vibration to **(L^{Ad}H)FeO$_2$**.

^{57}Fe Mössbauer measurements support a high-spin Fe(III) center in isolated **(L^{Ad}H)FeO$_2$**. The ^{57}Fe Mössbauer spectrum of polycrystalline **(L^{Ad}H)Fe** (Fig 2A) appears as a sharp quadrupole doublet with parameters ($\delta = 0.59$ mm/s, $\Delta E_Q = 1.45$ mm/s) in line with those of other low-coordinate, high-spin ferrous sites.[23,33] A spectrum

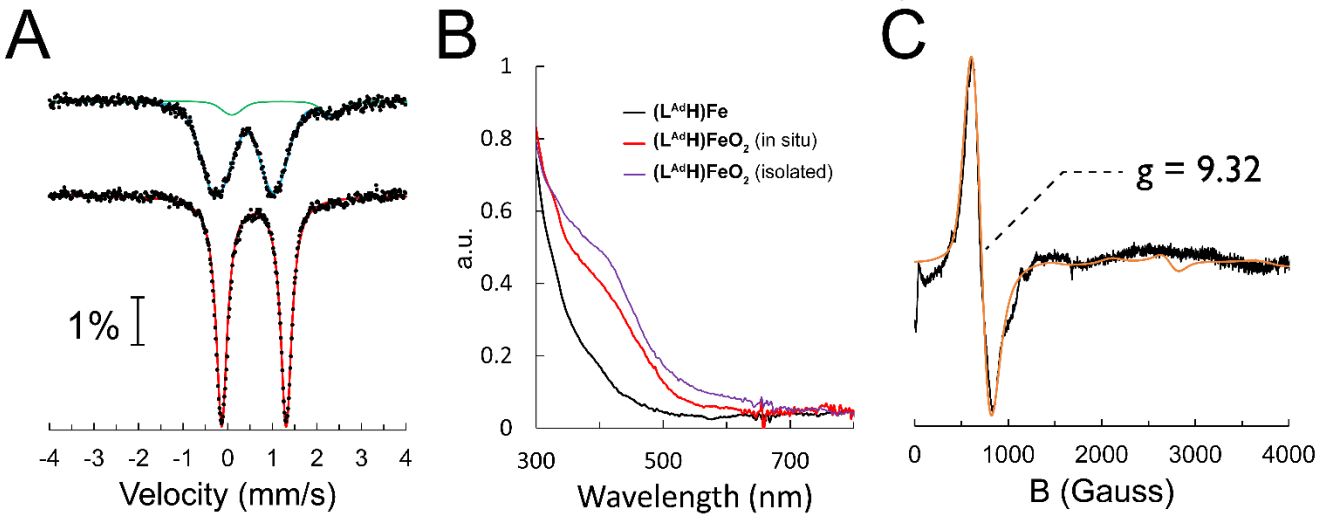

Figure 2. (A) Zero-field ^{57}Fe Mössbauer spectra of **(L^{Ad}H)Fe** (bottom) and **(L^{Ad}H)FeO$_2$** (top) collected at 80 K. A 10% Fe(II) impurity (green) is observed in the **(L^{Ad}H)FeO$_2$** sample. (B) UV-visible spectra of **(L^{Ad}H)Fe** (black) and **(L^{Ad}H)FeO$_2$** generated via *in situ* exposure to O_2 in toluene at -90 °C (red). The purple trace is the resulting spectra obtained following dissolution of isolated **(L^{Ad}H)FeO$_2$** powder in N_2-saturated toluene at -90 °C. (C) Parallel-mode X-band EPR spectrum of a toluene solution of **(L^{Ad}H)FeO$_2$** at 5 K and S_{TOT} = 2 simulation in orange. Refer to SI for simulation parameters.

obtained on similarly-prepared **(L^{Ad}H)Fe** material following O_2 exposure displays a single, broad quadrupole doublet with parameters (δ = 0.37 m/ms, ΔE_Q = 1.32 mm/s) consistent with a high-spin Fe(III) center in **(L^{Ad}H)FeO$_2$**.[34] The large linewidth associated with this spectrum may be a consequence of slow electronic relaxation at 80K, as suggested by EPR measurements (*vide infra*).

(L^{Ad}H)FeO$_2$ is readily prepared in solution phase. Exposure of yellow toluene solutions of **(L^{Ad}H)Fe** to dry O_2 results in the rapid development of a red color ascribed to **(L^{Ad}H)FeO$_2$** (Fig 2B). Dissolution of isolated, polycrystalline **(L^{Ad}H)FeO$_2$** gives rise to similar spectral features, supporting the notion that equivalent chemical species are generated upon oxygenation of **(L^{Ad}H)Fe** either in solution or as polycrystalline material. The magnitude of the extinction coefficients at 335 and 420 nm (~9000 and 6000 M^{-1} cm^{-1}, respectively) are suggestive of LMCT bands stemming from the phosphinimides and/or the O_2-derived ligand.[14] While the ^{1}H NMR spectrum of **(L^{Ad}H)Fe** consists of multiple sharp, paramagnetically-shifted peaks, *in situ*-generated **(L^{Ad}H)FeO$_2$** is NMR-silent (Fig S25). Solution-phase magnetic measurements of **(L^{Ad}H)Fe** recorded immediately ~1 min exposure to O_2 in C_6D_6 indicate an apparent S = 2 state for *in situ*-generated **(L^{Ad}H)FeO$_2$** at room temperature (μ_{eff} = 4.9 μ_B).

EPR studies were pursued to gain insight into the ground spin state of **(L^{Ad}H)FeO$_2$**. As previously discussed in detail for other non-heme iron-dioxygen complexes,[27-29,32] the interaction of O_2 with high-spin ferrous ions can give rise to Fe-O_2 complexes with total spin states (S_{TOT}) of 1, 2 or 3. Similar total spin states can be envisioned for **(L^{Ad}H)FeO$_2$**, the relative energies of which dictate the observed Boltzmann distribution at elevated temperatures. The parallel mode X-band EPR spectrum of **(L^{Ad}H)FeO$_2$** at 5 K contains an intense resonance at g = 9.32 (Fig 2C), similar to that observed in other synthetic[35] and enzymatic Fe-O_2 species.[4] This feature can be observed at temperatures up to 65 K and no other resonances emerge over this temperature range. This feature can be comparably simulated using S_{TOT} = 2 or 3 spin states attendant with rhombicity (E/D) values of 0.154 and 0.001, respectively (Fig S6). We favor the S_{TOT} = 2 simulation as **(L^{Ad}H)FeO$_2$** should exhibit substantial rhombic character owing to a distorted tetrahedral Fe geometry and aspherical metal-ligand π-bonding interactions.[36] Accordingly, we assign this resonance to a transition within the $|\pm2\rangle$ doublet of an energetically well-isolated S = 2 ground state.[37]

DFT methods provide further insight into the electronic structure of **(L^{Ad}H)FeO$_2$**. Gas-phase geometry optimizations were performed on modestly truncated **(L$^{t\text{-}Bu}$H)Fe** and **(L$^{t\text{-}Bu}$H)FeO$_2$** using the TPSSh functional.[38] Salient metrics found for gas-phase ^{5}**(L$^{t\text{-}Bu}$H)FeO$_2$** - specifically the Fe-N/O and O-O bond distances, Fe-O-O angle and local Fe geometry – closely match the experimental values found for **(L^{Ad}H)FeO$_2$** (Table S5). The natural orbitals constituting the Fe-O σ-interactions (Fig 3A) imply a delocalized 2-center-3-electron interaction of an Fe-d_{z^2} orbital and an O-O π^* orbital of the O_2-derived ligand. By convention, this interaction implies a formal reduction of O_2 to a O_2^- state. In contrast, the Fe-O π-interactions constructed from the bonding and antibonding combinations of an Fe-d_{xz} orbital and the orthogonal O-O π^* orbital exhibit non-integer electron occupancies. This situation implies a localized, antiferromagnetic interaction as the electron populations for these two orbitals sum to 2.0 electrons and the corresponding magnetic orbitals exhibit pronounced spatial overlap (Fig S26).[39] The magnitude of the exchange coupling constant predicted for this interaction (-58 to -136 cm^{-1})[40] corroborates a well-isolated ground spin state. Considering the three additional, singly-occupied orbitals (Fig S27), the electronic structure of ^{5}**(L$^{t\text{-}Bu}$H)FeO$_2$** is best described as an S = 5/2 Fe(III) center antiferromagnetically coupled to an S = 1/2 O_2^- ligand.

These computational studies also aid in rationalizing the apparent stability of **(L^{Ad}H)FeO$_2$**. The spin density plot for ^{5}**(L$^{t\text{-}Bu}$H)Fe** (Fig 3B) illustrates that the Fe center bears the majority of the unpaired electron density (+3.65 electrons) with minimal spin

leakage onto the two phosphinimide nitrogen atoms (+0.11 electrons total). In contrast, the spin density profile of **^{5}(L$^{t\text{-}Bu}$H)FeO$_2$** reveals substantial unpaired spin density on both the phosphinimide N-atoms (0.41 electrons total). Hence, electron density is mutually transferred from the Fe center and the supporting phosphinimides to O_2 upon its coordination. The cylindrical distribution of electron density on the N-atoms in **^{5}(L$^{t\text{-}Bu}$H)FeO$_2$** evidences Fe-N π-bonding interactions in two orthogonal planes. This situation contrasts that found for ligands commonly used to stabilize FeO_x species, such as porphyrin or amido-type (R_2N^-) donors, that are restricted to forming Fe-N π-bonds in a single orientation.[34,41,42] We hypothesize that the unique π-bonding characteristics of the **(L^{Ad}H)$^{2-}$** ligand serves to stabilize oxidized forms of bound metal ions, and in this case enables the robust coordination of O_2 to Fe.

The **(L^{Ad}H)Fe** platform engages in a range of oxidation reactions that proceed in stoichiometric and catalytic fashion. For example, **(L^{Ad}H)Fe** catalyzes the O_2-dependent conversion of 1,2-diphenylhydrazine to azobenzene (Fig 4A). The second order rate constants observed for azobenzene generation from ^{1}H- and ^{2}H-labeled 1,2-diphenylhydrazine implies a kinetic isotope effect of 4.9, consistent with a rate-determining hydrogen atom abstraction step that is presumably mediated by *in-situ* generated **(L^{Ad}H)FeO$_2$**. Under an O_2 atmosphere, **(L^{Ad}H)Fe** was found to quantitatively convert 1 equivalent of PPh_3 to $O{=}PPh_3$ over ~15 minutes (Fig 4B).[43] Isolated samples of **(L^{Ad}H)FeO$_2$** similarly react with PPh_3 under an N_2 atmosphere in benzene to afford a 74(1)% yield of $O{=}PPh_3$. The nature of the Fe-containing **(L^{Ad}H)Fe**-derived product(s) of these reactions are presently unknown and their characterization will be disclosed in a later report.

Finally, the **(L^{Ad}H)Fe** complex was found to catalyze C-C and C-H bond cleavage processes. Inspired by previous reports of nucleophilic metal-dioxygen species that engage in aldehyde deformylation,[7,44–49] we examined the reactivity of isolated **(L^{Ad}H)FeO$_2$** with 2-PPA. The stoichiometric combination of these compounds in benzene under an N_2 atmosphere resulted in the generation of acetophenone in 72(1)% yield. Interestingly, exposure of a 1:1 mixture of **(L^{Ad}H)Fe** and 2-PPA to 1 atm of O_2 resulted in the formation of acetophenone in >95% NMR yield. The identity of the other organic product was confirmed to be formic acid (Fig S2). Realizing that a full equivalent of dioxygen had been transferred to the substrate, we postulated that **(L^{Ad}H)Fe** could be regenerated upon deprotonation of the formic acid. Under ideal conditions that employ TBD as a base, 18 equiv of acetophenone are produced at 5 mol% **(L^{Ad}H)Fe** catalyst loading (Table 1). The direct usage of O_2 as an oxidant here is unusual,[46,49] and underscores the promising oxidation chemistry of the **(L^{Ad}H)Fe** system.

Table 1. (L^{Ad}H)Fe-catalyzed aldehyde deformylation

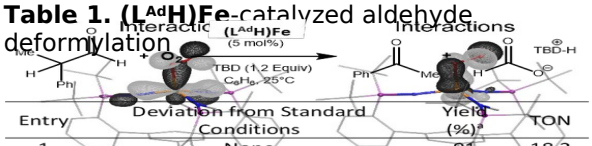

Conclusions

In summary, a non-heme Fe-O_2 complex has been prepared via exposure of O_2 to a phosphinimide-iron(II) compound. Its structural and spectroscopic features corroborate an antiferromagnetically-coupled, high-spin Fe(III)-superoxide site analogous to that predicted for many non-heme iron oxygenase enzymes. This amphoteric oxidant engages in both electrophilic O-atom transfer reactivity and nucleophilic aldehyde deformylation. These combined results demonstrate the utility in using phosphinimide ligands to simultaneously stabilize and harness reactive inorganic species. Further investigations aimed at probing the nature of the Fe-containing intermediates of these transformations are currently underway.

Experimental Section

General Considerations: Unless otherwise noted, all manipulations were carried out using standard Schlenk or glovebox techniques under an N_2 atmosphere. Acetonitrile (MeCN), Benzene, Diethyl ether (Et_2O), Pentane, Tetrahydrofuran (THF), and Toluene were deoxygenated by thoroughly sparging with N_2 gas followed by passing through an activated alumina column in a solvent purification system from Pure Process Technology, and were further dried over 4Å molecular sieves for 48h prior to use. Solvents were routinely tested with a THF solution of sodium benzophenone ketyl. Deuterated solvents were purchased from Cambridge Isotope Laboratories, Inc., and were distilled under N_2, degassed via freeze-pump-thaw cycles, and stored over 4Å molecular sieves prior to use. Oxygen was purchased in Ultra High Purity from Praxair and was further dried by passing through two traps immersed in a dry ice/isopropanol bath. All reagents were purchased from commercial vendors and used without further purification unless otherwise stated. 1,3,5-tris(2-bromophenyl)benzene[50], Di-(1-Adamantyl)Phosphine[51], O-(2,4-Dinitrophenyl)-N-hydroxyphthalimide[52], Fe(HMDS)$_2$[53], and d_2-diphenylhydrazine[54] were prepared according to literature procedures. Elemental analyses were performed by the Microanalytical Laboratory in the College of Chemistry at the University of California – Berkeley using a PerkinElmer 2400 Series II combustion analyzer.

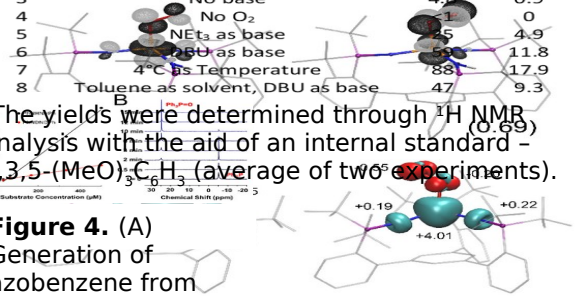

Figure 4. (A) Generation of azobenzene from 1,2-diphenylhydrazine (red) or d_2-1,2-diphenylhydrazine (blue) in the presence of $(L^{Ad}H)Fe$ and 1 atm O_2 at rt. (B) $^{31}P\{^1H\}$ NMR spectra illustrating the rt conversion of Ph_3P to $Ph_3P{=}O$-mediated by $(L^{Ad}H)Fe$ under 1 atm O_2.

Nuclear Magnetic Resonance: The yields were determined through ^1H NMR analysis with the aid of an internal standard – 1,3,5-$(MeO)_3C_6H_3$ (average of two experiments). Nuclear Magnetic Resonance (NMR) spectra were measured on a Varian 300 MHz or Agilent 400 MHz spectrometer. Chemical shifts are reported in ppm relative to tetramethylsilane (TMS) using the residual solvent peak as a reference. ^{31}P chemical shifts are reported relative to 85% H_3PO_4 as an external standard. Solution magnetic susceptibility measurements were obtained using the Evans method.[55]

Infrared Spectroscopy: Solid-state infrared (IR) measurements were obtained on a Nicolet iS20 Spectrometer as KBr pellets.

X-Ray Crystallography: XRD studies were performed at the Small Molecule X-Ray Crystallography Facility (CheXRay) of at beamline 12.2.1 at the Advanced Light Source at Lawrence Berkeley National Laboratory. For studies performed at ChexRay: Crystals were mounted on a Kapton loop under Paratone oil. Data were collected on a Rigaku XtaLAB P200 (MoKα or CuKα radiation) equipped with a MicroMax-007 HF microfocus rotating anode and a Pilatus 200K hybrid pixel array detector at 100 K under a stream of N_2. Data collection, integration and scaling were carried out using the CrysAlis[Pro] software.[56] For studies performed at the Advanced Light Source: Crystals were mounted on a MiTeGen loop under Paratone oil. Data were collected on a Bruker D85 phi three-circle diffractometer with a PHOTON II CCD area detector using silicon monochromated synchrotron radiation (λ = 0.7288 Å). Bruker APEX2 software was used for data collection. Bruker SAINT and SADABS software was utilized, for data reduction and absorption correction, respectively.[57,58] Structures were solved using SHELXS and refined against F^2 on all data by full matrix least-squared with SHELXL using OLEX2 crystallographic software.[59] All non-hydrogen atoms were refined using anisotropic displacement parameters. Hydrogen atoms were placed in idealized positions and refined using a riding model.

Electronic Paramagnetic Resonance Spectroscopy: X-band EPR spectra were obtained on a Bruker EMX spectrometer on 5 mM solutions as frozen glasses in toluene. Samples were collected at powers ranging from 1mW to 10mW and temperatures ranging from 5K to 65K with modulation amplitudes of 8 Gauss. Spectra were simulated using the EasySpin[60] suite of programs in Matlab 2021.

Optical Spectroscopy: Measurements were taken on a Hewlett-Packard 8453 UV-Vis Spectrophotometer using a 1cm quartz cell sealed with a Teflon stopcock. Variable Temperature measurements were performed using a UNISOKU Unispec Cryostat.

Electrochemistry: Electrochemical measurements were carried out in 0.2 M THF solutions of electrolyte ($[^nBu_4N][PF_6]$). Data collection were performed on a BioLogic SP-50 Potentiostat using a freshly-polished glassy carbon electron as the working electrode and a platinum wire as the auxiliary electrode. All reported potentials are referenced to the ferrocene/ferrocenium couple (Fc/Fc^+).

^{57}Fe Mössbauer Spectroscopy: Spectra were recorder on a spectrometer from SEE Co (Edina Mn) operating in the constant acceleration mode in a transmission geometry. The sample was kept in an SVT-400 cryostat from Janis (Wilmington, MA). The quoted isomer shifts are relative to the centroid of the spectrum of a metallic foil of a-Fe at room temperature. Samples were prepared by suspending polycrystalline material in an eicosane matrix and mounted in a Delrin cup fitted with a screw-cap. Data analysis was performed using the program WMOSS (www.wmoss.org) and quadrupole doublets were fit to either Lorentzian or Voigt line shapes.

DFT Calculations: All calculations were carried out using Gaussian 09 rev. D.01.[61] Coordinates for all heavy (non-H) atoms were taken from the structures determined via X-ray crystallography. To improve the efficiency of the calculations, the adamantyl substituents were truncated to tert-butyl substituents. Gas-phase geometry optimizations and single-point and frequency calculations employed the unrestricted TPSSH functional. The 6-31g(d) basis set was employed for C and H atoms and Def2-TZVPP was used for Fe, N, P and O atoms. Successful optimization to a minimum was confirmed by the absence of imaginary frequencies in a subsequent frequency calculation. Multireference character is expected for the S_{TOT} = 2 state of $(L^{t\text{-}Bu}H)FeO_2$ and a broken-symmetry solution is found via quadratically convergent SCF procedures. The resultant wavefunction was found to be the most stable using the "stable=opt" command. Natural orbitals were constructed using the pop=no command. Orbitals were visualized using VMD version 1.9.4a51.[62]

Synthesis of $(L^{Ad}H)Fe$: In the glove box, a 250 mL round-bottomed flask was charged with a magnetic stir bar, $L^{Ad}H_3$ (1.0g, 0.8 mmol, 1 Equiv), and Et_2O (60 mL). $Fe(HMDS)_2$ (296.0 mg, 0.8 mmol, 1 Equiv) was added dropwise to the flask as a solution in Et_2O (20 mL). The mixture was stirred for 24h resulting in a beige precipitate in a brown solution. The beige solid was collected on a medium frit and washed with Et_2O (3x15mL) to give $(L^{Ad}H)Fe$ as a beige powder (881.5 mg, 0.675 mmol, 84.5%). The filtrate was concentrated and stored at -30°C for 48h to obtain a second crop of $(L^{Ad}H)Fe$ (42.5 mg, 0.03 mmol, 4.1%) to give a combined yield of

88.6%. Single crystals of **(L^{Ad}H)**Fe suitable for X-ray diffraction were grown from layering pentane onto a concentrated Et_2O solution of **(L^{Ad}H)Fe** to give faint yellow rods. ^{1}H NMR (400 MHz, C_6D_6) δ 47.76, 41.88, 39.83, 36.47, 27.96, 22.19, 19.33, 16.27, 15.76, 15.16, 14.33, 13.06, 9.52, 8.42, 7.94, 6.03, 5.10, 3.60, 2.99, 2.71, 1.73, 1.33, 0.96, 0.18, -2.20, -2.71, -3.25, -3.74, -9.40, -11.02, -29.16, -45.23. Anal: calc. for $C_xH_yN_3P_3Fe$: C 77.22, H 8.18, N 3.22; found: C 75.74, H 8.20, N 3.01. μ_{eff} (Benzene-d_6, 298 K, 400 MHz): 4.94 μ_B. (KBr, 298 K, cm^{-1}): 3344 ν(*N-H)*.

Synthesis of (L^{Ad}H)FeO_2:

Method A: In-crystallo exposure to O_2

In the glove box, a 1-dram vial was charged with a suspension of crystalline **(L^{Ad}H)Fe** in an ether/pentane mother liquor and placed into a Schlenk tube. The tube was sealed with a glass stopper after briefly applying a mild vacuum to the headspace. The tube was subsequently transferred to a gas manifold and exposed to 1 atm of dry oxygen. Following ~90 min of O_2 exposure, visibly red crystals were mounted onto a diffractometer.

*Method B: Exposure of **(L^{Ad}H)Fe** powder to O_2*

In the glove box, a 1-dram vial was charged with **(L^{Ad}H)Fe** as a finely ground powder and placed into a Schlenk tube. The powder was completely dried in vacuo to remove all residual solvents. The tube was sealed with a glass stopper and transferred to a gas manifold under 1 atm of dry oxygen, resulting in an instant color change from beige to red. After 60 min exposure, the oxygen atmosphere was removed in vacuo and the Schlenk tube was transferred into a glove box for further manipulations.

*Method C: Exposure of **(L^{Ad}H)Fe** solutions to O_2*

In the glove box, a J-young tube or Schlenk bomb with a magnetic stir bar was charged with a solution of **(L^{Ad}H)Fe**. The vessel was sealed, removed from the glove box, and transferred to a gas manifold under 1 atm of dry oxygen. The solution was freeze-pump-thawed once before being exposed to oxygen to give a deep red solution of an NMR silent material. Modification for EPR samples: an EPR tube was charged with a 5 mM toluene solution of **(L^{Ad}H)Fe**, capped, and removed from the glove box before quickly being chilled in a dry ice/isopropanol bath. The tube was uncapped, and a long needle under positive pressure of O_2 was submerged in the solution for 10 seconds. The tube was quickly submersed in a liquid nitrogen bath to form a glass. Modification for UV-Vis: a Schlenk cuvette was charged with a 72 μM solution of **(L^{Ad}H)Fe**, sealed, and interted into a UNISOKU instrument precooled to -80 °C. Upon temperature equilibration, 1mL of dry O_2 was slowly injected into the cuvette.

In situ-generated C_6D_6 solutions of **(L^{Ad}H)FeO_2** prepared in this manner rapidly lose the paramagnetically shifted ^{1}H NMR features ascribed to **(L^{Ad}H)Fe** within minutes. Monitoring the magnetic moment of these solution by Evan's method reveals a negligible change in frequency shift (Fig S25). Over longer time periods, unidentified diamagnetic impurities begin to accumulate. Due to the instability of the compound in solution, reporting an accurate magnetic moment via this method would be difficult but the negligible frequency shift is consistent with an $S = 2$ species at room temperature. UV-Vis (Benzene, 298K, nm {$cm^{-1}M^{-1}$}): 335 {9200), 420(5900).

ASSOCIATED CONTENT

Experimental procedures, spectra and characterization data. This material is available free of charge via the Internet at http://pubs.acs.org.

AUTHOR INFORMATION

Corresponding Author

Jonathan Rittle – [0000-0001-6241-6253];
Email: rittle@berkeley.edu

Authors

Charles Winslow – [0000-0002-9296-1567]
Heui Beom Lee – [0000-0002-9550-2649]
Simon J. Teat – [0000-0001-9515-2602]
Mackenzie J. **Field**

Notes

The authors declare no competing financial interest.

ACKNOWLEDGMENT

This research was supported by the University of California Berkeley. X-ray diffraction experiments performed at beamline 12.2.1 at the Advanced Light Source at Lawrence Berkeley National Laboratory were supported by the Director, Office of Science, Office of Basic Energy Sciences, of the U.S. Department of Energy under Contract No. DE-AC02-05CH11231. We thank Prof Michael T. Green for access to a Mössbauer spectrometer, Prof R. David Britt and Dr. David Marchiori for access to and assistance with their EPR spectrometer (supported by NIH R35 Grant 1R35GM126961-01, to R.D.B), and Prof Christopher Chang for access to a Unisoku Cryostat. We thank Drs. Hasan Celik, Alicia Lund, and UC Berkeley's NMR facility in the College of Chemistry (CoC-NMR) for spectroscopic assistance. Instruments in the CoC-NMR are supported in part by NIH S10OD024998. M.J.F. was supported by a National Sciences and Engineering Research Council of Canada (NSERC) Postgraduate Scholarship.

ABBREVIATIONS

1,5,7-triazabicyclodecene (TBD)
1,8-Diazabicyclo(5.4.0)undec-7-ene (DBU)
2-Phenylpropionaldehyde (2-PPA)
Density Functional Theory (DFT)
Electronic Paramagnetic Resonance (EPR)

Ferrocene (Fc)

Fourier Transform Infrared (FTIR)
Hexamethyldisilazide (HMDS)
Nuclear Magnetic Resonance (NMR)
Triethylamine (NEt_3)
Turnover Number (TON) consistent
X-Ray Diffraction (XRD)

REFERENCES

(1) Shi, Z.; Zhang, C.; Tang, C.; Jiao, N. *Chem. Soc. Rev.* **2012**, *41* (8), 3381–3430.

(2) Costas, M.; Mehn, M. P.; Jensen, M. P.; Que, L. *Chem. Rev.* **2004**, *104* (2), 939–986.

(3) Peck, S. C.; van der Donk, W. A. *J. Biol. Inorg. Chem.* **2017**, *22* (2–3), 381–394.

(4) Mbughuni, M. M.; Chakrabarti, M.; Hayden, J. A.; Bominaar, E. L.; Hendrich, M. P.; Münck, E.; Lipscomb, J. D. *Proc. Natl. Acad. Sci. U. S. A.* **2010**, *107* (39), 16788–16793.

(5) Tamanaha, E.; Zhang, B.; Guo, Y.; Chang, W. C.; Barr, E. W.; Xing, G.; St Clair, J.; Ye, S.; Neese, F.; Bollinger, J. M.; Krebs, C. *J. Am. Chem. Soc.* **2016**, *138* (28), 8862–8874.

(6) Karlsson, A.; Parales, J. V.; Parales, R. E.; Gibson, D. T.; Eklund, H.; Ramaswamy, S. *Science (80-.).* **2003**, *299* (5609), 1039–1042.

(7) Hong, S.; Sutherlin, K. D.; Park, J.; Kwon, E.; Siegler, M. A.; Solomon, E. I.; Nam, W. *Nat. Commun.* **2014**, *5* (1), 1–7.

(8) Chiang, C. W.; Kleespies, S. T.; Stout, H. D.; Meier, K. K.; Li, P. Y.; Bominaar, E. L.; Que, L.; Münck, E.; Lee, W. Z. *J. Am. Chem. Soc.* **2014**, *136* (31), 10846–10849.

(9) Blakely, M. N.; Dedushko, M. A.; Yan Poon, P. C.; Villar-Acevedo, G.; Kovacs, J. A. *J. Am. Chem. Soc.* **2019**, *141* (5), 1867–1870.

(10) Oloo, W. N.; Que, L. *Acc. Chem. Res.* **2015**, *48* (9), 2612–2621.

(11) Collins, T. J. *Acc. Chem. Res.* **2002**, *35* (9), 782–790.

(12) White, M. C.; Doyle, A. G.; Jacobsen, E. N.; Har, V.; Uni, V.; March, R. V. **2001**, *2* (Ii), 7194–7195.

(13) Chen, M. S.; White, M. C. *Science (80-.).* **2010**, *327* (5965), 533–571.

(14) Lee, H. B.; Ciolkowski, N.; Winslow, C.; Rittle, J. *No Title*.

(15) Dehnicke, K.; Krieger, M.; Massa, W. *Coord. Chem. Rev.* **1999**, *182* (1), 19–65.

(16) Stephan, D. W. *Organometallics* **1999**, *18* (7), 1116–1118.

(17) Rice, N. T.; Popov, I. A.; Russo, D. R.; Bacsa, J.; Batista, E. R.; Yang, P.; Telser, J.; La Pierre, H. S. *J. Am. Chem. Soc.* **2019**, *141* (33), 13222–13233.

(18) Scepaniak, J. J.; Harris, T. D.; Vogel, C. S.; Sutter, J.; Meyer, K.; Smith, J. M. *J. Am. Chem. Soc.* **2011**, *133* (11), 3824–3827.

(19) Camacho-Bunquin, J.; Ferguson, M. J.; Stryker, J. M. *J. Am. Chem. Soc.* **2013**, *135* (15), 5537–5540.

(20) Eckert, N. A.; Smith, J. M.; Lachicotte, R. J.; Holland, P. L. *Inorg. Chem.* **2004**, *43* (10), 3306–3321.

(21) Maddock, L. C. H.; Cadenbach, T.; Kennedy, A. R.; Borilovic, I.; Aromí, G.; Hevia, E. *Inorg. Chem.* **2015**, *54* (18), 9201–9210.

(22) Margraf, G.; Schödel, F.; Sänger, I.; Bolte, M.; Wagner, M.; Lerner, H. W. *Zeitschrift fur Naturforsch. - Sect. B J. Chem. Sci.* **2012**, *67* (6), 549–556.

(23) Sazama, G. T.; Betley, T. A. *Inorg. Chem.* **2010**, *49* (5), 2512–2524.

(24) Höpfl, H. *J. Organomet. Chem.* **1999**, *581* (1–2), 129–149.

(25) XRD analysis of four independently prepared crystals of **$(L^{Ad}H)FeO_2$** reveal consistent metrics for the $\{FeO_2\}$ unit that corroborate substantial reduction of the O_2 ligand upon coordination. The metrics discussed here represent the data set which exhibited superior crystallographic statistics. See Supporting Information for further details.

(26) Kumar, D.; Thiel, W.; De Visser, S. P. *J. Am. Chem. Soc.* **2011**, *133* (11), 3869–3882.

(27) Bassan, A.; Borowski, T.; Siegbahn, P. E. M. *Dalt. Trans.* **2004**, No. 20, 3153–3162.

(28) Ye, S.; Riplinger, C.; Hansen, A.; Krebs, C.; Bollinger, J. M.; Neese, F. *Chem. - A Eur. J.* **2012**, *18* (21), 6555–6567.

(29) Coggins, M. K.; Sun, X.; Kwak, Y.; Solomon, E. I.; Rybak-Akimova, E.; Kovacs, J. A. *J. Am. Chem. Soc.* **2013**, *135* (15), 5631–5640.

(30) Dehnicke, K.; Strähle, J. *Polyhedron* **1989**, *8* (6), 707–726.

(31) Creutz, S. E.; Peters, J. C. *Inorg. Chem.* **2016**, *55* (8), 3894–3906.

(32) Alecu, I. M.; Zheng, J.; Zhao, Y.; Truhlar, D. G. *J. Chem. Theory Comput.* **2010**, *6* (9), 2872–2887.

(33) Macdonnell, F. M.; Ruhlandt-senge, K.; Ellison, J. J.; Holm, R. H.; Power, P. P. **1995**, No. Ii, 1815–1822.

(34) MacBeth, C. E.; Golombek, A. P.; Young, J.; Yang, C.; Kuczera, K.; Hendrich, M. P.; Borovik, A. S. *Science (80-.).* **2000**, *289* (5481), 938–941.

(35) Stout, H. D.; Kleespies, S. T.; Chiang, C. W.; Lee, W. Z.; Que, L.; Münck, E.; Bominaar, E. L. *Inorg. Chem.* **2016**, *55* (11), 5215–5226.

(36) Sazama, G. T.; Betley, T. A. *Inorg. Chem.* **2014**, *53* (1), 269–281.

(37) Kostka, K. L.; Fox, B. G.; Collins, T. J.; Münck, E.; Hendrich, M. P.; Rickard, C. E. F.; Wright, L. J. *J. Am. Chem. Soc.* **1993**, *115* (15), 6746–6757.

(38) Jensen, K. P. *Inorg. Chem.* **2008**, *47* (22), 10357–10365.

(39) Woertink, J. S.; Tian, L.; Maiti, D.; Lucas, H. R.; Himes, R. A.; Karlin, K. D.; Neese, F.; Würtele, C.; Holthausen, M. C.; Bill, E.; Sundermeyer, J.; Schindler, S.; Solomon, E. I. *Inorg. Chem.* **2010**, *49* (20), 9450–9459.

(40) Tomson, N. C.; Crimmin, M. R.; Petrenko, T.; Rosebrugh, L. E.; Sproules, S.; Christopher Boyd, W.; Bergman, R. G.; Debeer, S.; Dean Toste, F.; Wieghardt, K. *J. Am. Chem. Soc.* **2011**, *133* (46), 18785–18801.

(41) Schappacher, M.; Weiss, R.; Montiel-Montoya, R.; Trautwein, A.; Tabard, A. *J. Am. Chem. Soc.* **1985**, *107* (12), 3736–3738.

(42) De Oliveira, F. T.; Chanda, A.; Banerjee, D.; Shan, X.; Mondal, S.; Que, L.; Bominaar, E. L.; Münck, E.; Collins, T. J. *Science (80-.).* **2007**, *315* (5813), 835–838.

(43) Cho, J.; Woo, J.; Nam, W. *J. Am. Chem. Soc.* **2012**, *134* (27), 11112–11115.

(44) Wertz, D. L.; Valentine, J. S. In *Metal-Oxo and Metal-Peroxo Species in Catalytic Oxidations*; Meunier, B., Ed.; Springer Berlin Heidelberg: Berlin, Heidelberg, 2000; pp 37–60.

(45) Shokri, A.; Que, L. *J. Am. Chem. Soc.* **2015**, *137* (24), 7686–7691.

(46) Annaraj, J.; Suh, Y.; Seo, M. S.; Kim, S. O.; Nam, W.

Chem. Commun. **2005**, No. 36, 4529–4531.

(47) Lin, Y. H.; Kutin, Y.; Van Gastel, M.; Bill, E.; Schnegg, A.; Ye, S.; Lee, W. Z. *J. Am. Chem. Soc.* **2020**, *142* (23), 10255–10260.

(48) Cho, J.; Sarangi, R.; Annaraj, J.; Kim, S. Y.; Kubo, M.; Ogura, T.; Solomon, E. I.; Nam, W. *Nat. Chem.* **2009**, *1* (7), 568–572.

(49) Corcos, A. R.; Villanueva, O.; Walroth, R. C.; Sharma, S. K.; Bacsa, J.; Lancaster, K. M.; MacBeth, C. E.; Berry, J. F. *J. Am. Chem. Soc.* **2016**, *138* (6), 1796–1799.

(50) Hillenbrand, J.; Leutzsch, M.; Yiannakas, E.; Gordon, C. P.; Wille, C.; Nöthling, N.; Copéret, C.; Fürstner, A. *J. Am. Chem. Soc.* **2020**, *142* (25), 11279–11294.

(51) Goerlich, J. R.; Schmutzler, R. *Phosphorus. Sulfur. Silicon Relat. Elem.* **1995**, *102* (1–4), 211–215.

(52) Legault, C.; Charette, A. B. *J. Org. Chem.* **2003**, *68* (18), 7119–7122.

(53) Broere, D. L. J.; Čorić, I.; Brosnahan, A.; Holland, P. L. *Inorg. Chem.* **2017**, *56* (6), 3140–3143.

(54) Sadique, A. R.; Gregory, E. A.; Brennessel, W. W.; Holland, P. L. *J. Am. Chem. Soc.* **2007**, *129* (26), 8112–8121.

(55) Evans, D. F. *J. Chem. Soc.* **1959**, *0* (0), 2003.

(56) Rigaku Oxford Diffraction. Rigaku Corporation: Oxford, U.K. 2015.

(57) Bruker AXS Inc.: Madison, WI 2014.

(58) Sheldrick, G. Bruker Analytical X-Ray Systems, Inc.: Madison, WI 2000.

(59) Dolomanov, O. V.; Bourhis, L. J.; Gildea, R. J.; Howard, J. A. K.; Puschmann, H. *J. Appl. Crystallogr.* **2009**, *42* (2), 339–341.

(60) Stoll, S.; Schweiger, A. *J. Magn. Reson.* **2006**, *178* (1), 42–55.

(61) Frisch, M. J.; Trucks, G. W.; Schlegel, H. B.; Scuseria, G. E.; Robb, M. A.; Cheeseman, J. R.; Scalmani, G.; Barone, V.; Mennucci, B.; Petersson, G. A.; Nakatsuji, H.; Caricato, M.; Li, X.; Hratchian, H. P.; Izmaylov, A. F.; Bloino, J.; Zheng, G.; Sonnenberg, J. L.; Hada, M.; Ehara, M.; Toyota, K.; Fukuda, R.; Hasegawa, J.; Ishida, M.; Nakajima, T.; Honda, Y.; Kitao, O.; Nakai, H.; Vreven, T.; J. A. Montgomery, J.; Peralta, J. E.; Ogliaro, F.; Bearpark, M.; Heyd, J. J.; Brothers, E.; Kudin, K. N.; Staroverov, V. N.; Keith, T.; Kobayashi, R.; Normand, J.; Raghavachari, K.; Rendell, A.; Burant, J. C.; Iyengar, S. S.; Tomasi, J.; Cossi, M.; Rega, N.; Millam, J. M.; Klene, M.; Knox, J. E.; Cross, J. B.; Bakken, V.; Adamo, C.; Jaramillo, J.; Gomperts, R.; Stratmann, R. E.; Yazyev, O.; Austin, A. J.; Cammi, R.; Pomelli, C.; Ochterski, J. W.; Martin, R. L.; Morokuma, K.; Zakrzewski, V. G.; Voth, G. A.; Salvador, P.; Dannenberg, J. J.; Dapprich, S.; Daniels, A. D.; Farkas, O.; Foresman, J. B.; Ortiz, J. V; Cioslowski, J.; Fox, D. J. Gaussion Inc.: Wallingford CT 2013.

(62) Humphrey, W.; Dalke, A.; Schulten, K. *J. Mol. Graph.* **1996**, *14* (1), 33–38.

Table of Contents Graphic